Elastic collisions of interstellar helium atoms with solar wind protons

Mike Gruntman[1]

Received 24 November 2012; revised 27 January 2013; accepted 20 February 2013.

[1] Relative motion of the Sun with respect to the surrounding local interstellar medium results in entering of interstellar helium atoms into the heliosphere. Current models of helium flowing into the solar system do not include elastic collisions of atoms with solar wind ions. It was predicted in 1986, without quantitative elaboration, that such collisions would enhance wings of directional distributions of helium atom fluxes. This paper focuses on a theoretical treatment of elastic collisions of interstellar He atoms with the solar wind protons resulting in increased wing intensities, called the helium flux halo in contradistinction to the flux core. We concentrate on directional distributions of He atom intensities at 1 AU from the Sun for observers at rest and moving with the Earth and confirm the formation of the flux halo. We show that the collision-produced halo would often dominate He atom intensities at angles larger than 30°–35° from the maximum intensity direction in the flux core. A comparison with direct measurements of interstellar helium atom fluxes is beyond the scope of this paper.

Citation: Gruntman, M. (2013), Elastic collisions of interstellar helium atoms with solar wind protons, *J. Geophys. Res. Space Physics*, *118*, doi:10.1002/jgra.50199.

1. Interstellar Helium in the Solar System

[2] Relative motion of the Sun with respect to the surrounding partially ionized local interstellar medium (LISM) results in entering of interstellar neutral helium atoms into the heliosphere. The low number density of LISM's interstellar gas justifies treating these atoms as individual particles moving along hyperbolic trajectories under the gravitational force of the Sun and experiencing ionization losses. More than 40 years of extensive experimental studies support the concept of interstellar helium penetration of the solar system. The techniques include optical (interplanetary glow) and in situ (pickup ions and direct flux detection) measurements [e.g., *Moebius et al*., 2004, and references therein].

[3] Optical observations and pickup ion measurements essentially average out properties of neutral interstellar helium over large distances in the heliosphere. In contrast, direct detection of He atom fluxes measures local directional distributions of atom intensities (cm^{-2} sr^{-1} s^{-1}), sometimes also called directional fluxes. These distributions depend on the velocity, temperature, and number density of helium "at infinity" in the interstellar medium surrounding the Sun thus characterizing LISM properties.

[4] Direct detection of interstellar He atom fluxes played an important role in emergence of a new field of in situ measurements of neutral atoms in the solar system [*Gruntman*, 1997]. An experiment GAS [*Rosenbauer et al*., 1983; *Witte et al*., 1992] onboard the Ulysses spacecraft, launched in 1990, successfully detected for the first time interstellar helium fluxes [*Witte et al*., 1996; *Witte*, 2004]. Then, the Interstellar Boundary Explorer (IBEX) [*McComas et al*., 2009], launched in 2008, measured interstellar helium fluxes at 1 AU [*Moebius et al*., 2009a]. In situ measurements of low energy neutral atoms (50–120 eV in case of interstellar helium) utilize various experimental approaches [*Gruntman*, 1993, 1997]. The instruments on Ulysses [*Rosenbauer et al*., 1983; *Witte et al*., 1992, 1999] and IBEX [*Moebius et al*., 2009b], based on different physical detection processes, obtained interstellar helium properties that are in general agreement [*Witte*, 2004; *Bzowski et al*., 2012; *Moebius et al*., 2012], although some differences are not explained yet.

[5] The dynamics of interstellar helium atom motion in the gravitational field of the Sun and atom losses are well understood. Recent IBEX measurements revealed higher intensities in the wings of interstellar helium directional distributions than predicted by conventional theoretical models [*Bzowski et al*., 2012; *Moebius et al*., 2012]. *Bzowski et al*. [2012] suggested that these enhanced wings were "likely produced by interaction of interstellar helium with plasma in the outer heliosheath" which could result in effectively non-Maxwellian velocity distributions of the inflowing interstellar helium at large distances (>100 AU) from the Sun.

[6] There is another physical effect however that would enhance wing intensities which we call the helium flux halo in contradistinction to the well-understood helium flux core. *Brandt* [1964] first pointed to the importance of elastic and

[1]Department of Astronautical Engineering, Viterbi School of Engineering, University of Southern California, Los Angeles, California, USA.

Corresponding author: M. Gruntman, Department of Astronautical Engineering, Viterbi School of Engineering, University of Southern California, Los Angeles, CA 90089-1192, USA. (mikeg@usc.edu)

2169-9380/13/10.1002/jgra.50199

inelastic collisions of interstellar atoms with the solar wind protons and electrons. It had been realized by mid-1970s that elastic collisions might cause effective heating of the inflowing interstellar atom fluxes [*Wallis*, 1973; *Fahr*, 1974; *Holzer*, 1977; *Meier*, 1977]. By mid-1980s, a number of authors [*Fahr and Lay*, 1974; *Wallis*, 1974, 1975; *Fahr* 1978; *Wallis and Hassan*, 1978; *Wu and Judge*, 1978; *Chassefiere et al*., 1986; *Gruntman*, 1986] had explored various aspects of such heating of interstellar helium and hydrogen.

[7] Collisional heating of interstellar helium was initially often treated as accumulation of momentum- and energy-transfer processes continuously occurring along atom trajectories to a point of interest in the heliosphere. The net momentum (energy) transfer was essentially determined as a product of the average momentum (energy) transferred in a collision and the average number of such collisions.

[8] Then, *Gruntman* [1986] noted that the concept of continuous momentum and energy transfer was inapplicable because of the small average number of collisions. (In contrast to long-range Coulomb forces between charged particles in plasma, ion-neutral interaction potentials are essentially short-range which limits total cross-sections, with rapidly diminishing contribution of collisions at large impact parameters.) The analysis of differential scattering cross-sections, sharply peaking at small scattering angles, pointed to a fundamental inequality of transferred momentum (energy) among atoms experiencing collisions. (*Chassefiere et al.* [1986] also independently arrived at similar conclusions.) Most He atoms would acquire in one collision only small, compared to the average, additional momentum and energy while a few atoms obtain significant momentum and energy increments. Consequently, *Gruntman* [1986] specifically predicted that collision-produced widening (heating) of the core of directional distributions of He atom fluxes at 1 AU would be small and could probably "be neglected in treatment of direct experimental data" and that a small fraction of atoms would produce "very thin (but rather long) wings in the interstellar helium velocity distribution function." These predictions have not been further quantitatively elaborated at that time.

[9] This paper theoretically describes elastic collisions of interstellar He atoms with the solar wind protons leading to effective heating of interstellar helium and forming the flux halo. We quantitatively assess the effect and confirm the earlier prediction by *Gruntman* [1986]. The calculated He atom flux halo at 1 AU would contribute to and could explain some observed intensity enhancements [*Moebius et al*., 2012; *Bzowski et al*., 2012] in the wings of directional distributions of interstellar helium fluxes.

[10] Section 2 of the paper briefly reviews the conventional (without collisions) theoretical treatment of interstellar atoms flowing into the heliosphere and local properties of He atom fluxes. Then, section 3 considers elastic collisions between solar wind protons and helium atoms. Section 4 describes the effect of elastic collisions on local velocity distributions and presents the calculated He flux halo at 1 AU for observers at rest and moving with the Earth. Finally, section 5 summarizes the results and discusses effects of the simplifying assumptions made in this work on accuracy of the halo calculations. A comparison of the presented theoretical results with measurements of interstellar helium atom fluxes is beyond the scope of this publication and will be done in the future.

2. Interstellar Helium Atom Fluxes

[11] Let us first consider a conventional treatment of inflowing interstellar helium without elastic collisions with the solar wind protons. *Danby and Camm* [1957], *Danby and Bray* [1967], and *Fahr* [1968, 1971] first introduced basic concepts of interstellar neutral atom penetration of the solar system that essentially relied on conservation of the phase space density along particle trajectories. These concepts laid the foundation for various approaches developed in the 1970s for obtaining local distribution functions of interstellar hydrogen and helium atoms [e.g., *Axford*, 1972; *Fahr*, 1974, 1979; *Wallis*, 1974; *Weller and Meier*, 1974; *Blum et al*., 1975; *Holzer*, 1977; *Meier*, 1977; *Wu and Judge*, 1979; *Thomas*, 1978; *Gruntman*, 1980]. Later, a number of groups applied these approaches in diverse studies of interstellar neutral gas in the heliosphere [e.g., *Bertaux*, 1984; *Lallement et al*., 1985; *Fahr et al*., 1987; *Banaszkiewicz et al*., 1990, 1996; *Hall et al*., 1993; *Quemerais and Bertaux*, 1993; *Ajello et al*., 1994; *Witte et al*., 1996; *Pryor et al*., 1998, 2008; *Quemerais et al*., 1999; *Stephan et al*., 2001; *Rucinski et al*., 2003; *Moebius et al*., 2004, 2009a, 2012; *Tarnopolski and Bzowski*, 2009; *Katushkina and Izmodenov*, 2011; *Bzowski et al*., 2012; *Lee et al*., 2012].

[12] Interstellar helium atoms enter the solar system and follow heliocentric hyperbolic trajectories under the influence of the gravitational field of the Sun (Figure 1). (Effective solar radiation forces caused by atom scattering of solar photons do not exceed a fraction of one half of one percent of the gravitational force and can be conveniently disregarded.) An atom with the initial velocity vector $\mathbf{V_1}$ at infinity in the LISM would have the velocity $\mathbf{V}$ at a selected point $\mathbf{R}$ in the heliosphere; the angle θ^* describes an angular position of the atom along the hyperbolic

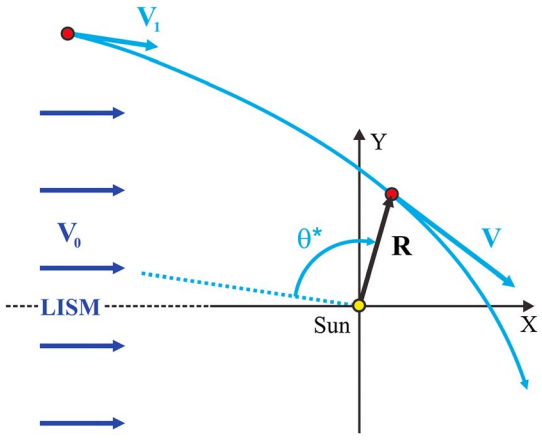

Figure 1. An interstellar helium atom entering the heliosphere. $\mathbf{V_1}$ is the atom velocity vector "at infinity" in the LISM; $\mathbf{V}$ is the atom velocity at a given point $\mathbf{R}$; $\mathbf{V_0}$ is the LISM velocity (interstellar wind) with respect to the Sun, its vector pointing in the x axis direction; the angle $\boldsymbol{\theta}^*$ describes an angular position of the atom along its hyperbolic trajectory and is measured from the incoming radial asymptote (dotted line). The Sun, the LISM velocity $\mathbf{V_0}$, and the radius-vector $\mathbf{R}$ are in the plane of the figure; vectors $\mathbf{V}$ and $\mathbf{V_1}$ are not necessarily in the plane.

trajectory. This angle is measured from the incoming radial asymptote of the hyperbola that is from the direction opposite to the vector $\mathbf{V_1}$ (Figure 1). (In contrast, true anomaly which is commonly used for describing a point position is counted from perihelion.)

[13] In the absence of atom losses, the phase space density of interstellar helium is conserved along particle trajectories, as required by the Liouville's theorem [e.g., *Landau and Lifshitz*, 1976; *Goldstein*, 1980]. Consequently, the phase space density $f(\mathbf{V},\mathbf{R})$ at the selected point $\mathbf{R}$ equals the phase space density $f_1(\mathbf{V_1})$ of atoms in the LISM:

$$f(\mathbf{V},\mathbf{R}) = f_1(\mathbf{V_1}), \tag{1}$$

where the local velocity vector $\mathbf{V}$ and the radius-vector $\mathbf{R}$ determine the velocity vector $\mathbf{V_1}$ at infinity, $\mathbf{V_1}=\mathbf{V_1}(\mathbf{V},\mathbf{R})$. The problem of calculating a local velocity distribution function at a given point is thus reduced to accounting for losses and determining velocities $\mathbf{V_1}$ in the interstellar gas for the given local $\mathbf{V}$ and $\mathbf{R}$. The latter calculations are common in orbital mechanics [e.g., *Battin*, 1987; *Vallado*, 2001, and references therein].

[14] One usually assumes a shifted Maxwellian velocity distribution of neutral atoms in the LISM's interstellar gas approaching the solar system:

$$f_1(\mathbf{V_1}) = n_0\left(\frac{m_{\mathrm{He}}}{2\pi k_B T_0}\right)^{3/2}\exp\left[-\frac{m_{\mathrm{He}}}{2k_B T_0}(\mathbf{V_0}-\mathbf{V_1})^2\right], \tag{2}$$

where n_0 is the helium number density in the LISM, m_{He} is the helium atom mass; k_B is the Boltzmann constant; T_0 is the LISM temperature; and $\mathbf{V_0}$ is the interstellar gas bulk velocity vector ("interstellar wind" velocity) with respect to the Sun. For a realistic interstellar gas temperature, such as 8000 K, the corresponding root-mean-square velocity of helium atom thermal motion in a selected direction is 4.1 km s^{-1}, which is smaller but not negligible than a realistic interstellar wind velocity of 25 km s^{-1}. Hence, the spread of helium atom velocities in the LISM would result in directional dependences of local interstellar helium atom intensities in the heliosphere.

[15] In this work, we concentrate on properties of interstellar helium fluxes along the Earth orbit which are of most interest for realistic space experiments. The interstellar wind velocity vector $\mathbf{V_0}$ points in the direction close to the ecliptic plane with ecliptic latitude $\beta_{\mathrm{ISW}} \approx -5°$. We make two simplifying assumptions that (i) the interstellar wind vector is in the ecliptic plane and (ii) the observer is at rest in the circular Earth orbit around the Sun with the radius $R_E = 1$ AU. One can generalize the treatment in a straightforward manner for any location in the heliosphere, any interstellar wind velocity, and any velocity of an observing platform. In section 4, we present, as an example, a directional distribution of He atom intensities for a realistic interstellar wind velocity vector and an observer moving with the Earth. Throughout this work, we assume the LISM velocity $V_0 = 25$ km s^{-1} with respect to the Sun, temperature $T_0 = 8000$ K, and the helium atom number density $n_0 = 0.01$ cm^{-3}.

[16] Let us consider, as was suggested by *Fahr* [1968], interstellar atoms approaching the solar system with the same velocities V_0 and from the same direction (Figure 2). This is a so-called "cold model" of the interaction, with the zero temperature of the interstellar gas. (A "hot model" refers to a non-zero LISM temperature.) It is convenient to describe the coordinates of a selected "observation point" in the heliocentric system of coordinates, $\mathbf{R}=(R,\theta)$, with the position angle θ counted from the direction opposite to the velocity vector $\mathbf{V_0}$, that is, from the upwind (interstellar wind) direction. We will use henceforth the symbol θ to describe angular positions of observers in the heliocentric system and the same symbol with the asterisk, θ^*, to describe angular positions of atoms along their hyperbolic trajectories, measured from the incoming radial asymptote (Figure 1). The angles θ and θ^* are identical when $\mathbf{V_0}=\mathbf{V_1}$, that is, for the cold model.

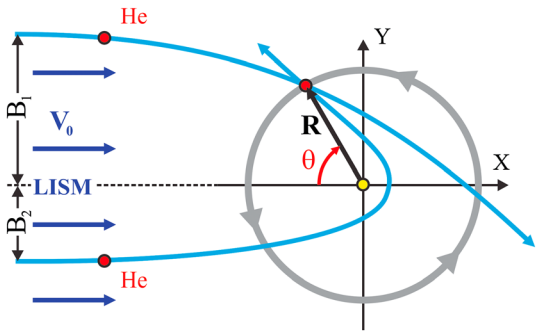

Figure 2. Interstellar helium atoms reaching a given point $\mathbf{R}=(R,\theta)$ in the heliosphere along two distinctly different trajectories with impact parameters $\boldsymbol{B_1}$ (direct trajectories) and $\boldsymbol{B_2}$ (indirect trajectories). The position angle $\boldsymbol{\theta}$ is measured from the upwind (interstellar wind $\mathbf{V_0}$) direction (that is, from the negative direction of the x axis). The gray circle is the Earth orbit if $\boldsymbol{R}=\boldsymbol{R_E}$ and arrows show the direction of counterclockwise Earth motion.

[17] Figure 2 shows interstellar atoms reaching any given point (R,θ) in the heliosphere following two distinctly different trajectories with two different "impact parameters," B_1 (with $\theta^*=\theta$) and B_2 (with $\theta^*=360°-\theta$). An atom trajectory reaching a given point with the angle $\theta^*<180°$ from the incoming radial asymptote is referred to as direct while a trajectory with $\theta^*>180°$ is indirect. For the selected interstellar wind velocity 25 km s^{-1}, a point $\theta \approx 126°$ at the Earth orbit is unique and of special interest for experiments. The corresponding direct atom trajectory is tangential to the circular Earth orbit at this point (atom orbit perihelion). Consequently, interstellar helium atoms would have at this point the highest velocities relative to the moving Earth (revolving around the Sun in the counterclockwise direction in Figure 2) which is especially advantageous for atom direct detection from an Earth-bound spacecraft [*Gruntman*, 1980, 1993; *McComas et al.*, 2009; *Moebius et al.*, 2009a, 2009b]. Another direct trajectory would tangentially "touch" the Earth orbit below the axis of symmetry in Figure 2 at $\theta \approx 234°$. The velocities of helium atoms with respect to the moving Earth would be minimal at that point, making it unfavorable for atom direct detection.

[18] On its trajectory from the LISM to a given point, an atom may get ionized and thus lost. Loss rates due to photo-ionization and solar wind ion charge exchange are inversely proportional to the square of the heliocentric distance. The dominating loss process is photo-ionization by the solar extreme ultraviolet radiation. The photo-ionization rate varies from 6×10^{-8} to 1.7×10^{-7} s^{-1} at 1 AU from solar minimum to solar maximum, respectively [*McMullin*

et al., 2004]. Helium loss due to charge exchange with solar wind ions does not exceed 7% of photo-ionization.

[19] The typical solar wind electron impact ionization rate is about 2.0×10^{-8} s^{-1} at 1 AU, or about one third and one eighth of photo-ionization during solar minimum and solar maximum, respectively [*McMullin et al.*, 2004]. The relative importance of electron impact ionization increases with decreasing heliocentric distance due to larger electron temperatures in the solar wind near the Sun. For direct helium atom trajectories reaching 1 AU, the electron impact ionization always remains significantly smaller than photo-ionization.

[20] We assume in this work the isotropic effective helium atom loss (ionization) rate $\eta(R)$:

$$\eta(R) = \eta_E \left(\frac{R_E}{R}\right)^2, \tag{3}$$

where $\eta_E = \eta(R_E)$ is the ionization rate at 1 AU from the Sun. The probability P_0 for an atom to reach a point (R,θ^*) without being lost to ionization, the survival probability, is an integral along the hyperbolic trajectory from infinity:

$$P_0(R,\theta^*) = \exp\left[-\int \eta(t)\,\mathrm{d}t\right]. \tag{4}$$

[21] Using conservation of specific angular momentum, $h_0 = R^2\dot{\theta}^*$, along the atom trajectory and substituting integration over the angle θ^* for that over time, one obtains

$$P_0(R,\theta^*) = \exp\left[-\frac{\eta_E R_E^2}{h_0}\theta^*\right]. \tag{5}$$

[22] Note that $\theta = \theta^*$ and $P_0(R,\theta) = P_0(R,\theta^*)$ for the cold model. For the hot model describing a realistic interstellar gas with non-zero temperature, the He atom intensity at a selected point (R,θ) would peak in the direction corresponding to interstellar atoms with the velocity $\mathbf{V_0}$ in the LISM (that is with the zero thermal velocity and $\theta = \theta^*$). The survival probability (and the average number of elastic collisions, as we show below) depends on the angle from the incoming asymptote θ^*, and it would thus vary for He atoms arriving from different directions to the selected point. Therefore, equation (5) describes the survival probability of atoms at a peak intensity of directional distributions at a given point (R,θ) by substituting the position angle θ.

[23] Figure 3 shows the survival probability P_0 dependence on the position angle θ at the Earth orbit for the cold model (or, generally, on the angle from the incoming asymptote θ^*) for an effective He atom loss rate $\eta_E = 1.0 \times 10^{-7}$ s^{-1}. For direct trajectories, the survival probability decreases from 0.67 in the upwind direction ($\theta = 0°$) down to 0.33 in the downwind direction ($\theta = 180°$). At $\theta \approx 126°$, an important point for experimental observations, the survival probability is $P_0 \approx 0.51$. The probabilities are much smaller for atoms in indirect trajectories, e.g., 0.10 for $\theta = 240°$ and 0.0023 for $\theta = 300°$. In addition, the disregarded relative increase of electron impact ionization within 1 AU would further diminish survival probabilities of such atoms. Higher losses on indirect trajectories make them less favorable for observations.

[24] We use the survival probability dependence $P_0(R,\theta^*)$ (equation (5)) along individual atom trajectories to account for interstellar He atom losses in calculations, based on equation (1), of local velocity distribution functions. Then we integrate the latter over velocity magnitudes in selected directions to obtain the interstellar helium atom intensities (cm^{-2} sr^{-1} s^{-1}) from these directions. The experiments on Ulysses and IBEX measured directional distributions of interstellar helium intensities.

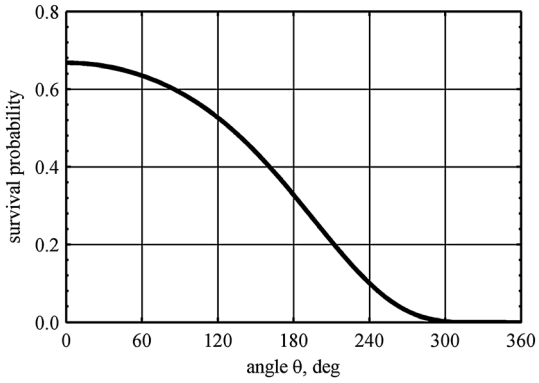

Figure 3. Interstellar He atom survival probability for reaching 1 AU as a function of the position angle θ for the cold model (or, generally, a function of the angle from the incoming asymptote θ^*). The initial atom velocity in the LISM is $V_0 = 25$ km s^{-1} and the loss rate is $\eta_E = 10^{-7}$ s^{-1} at 1 AU.

[25] Figure 4 shows the calculated all-sky interstellar He atom intensity maps for an observer at rest at three points (Figure 4a) at the Earth orbit: $\theta = 0°$ (upwind direction; Figure 4b), $\theta = 126°$ (perihelion of the corresponding direct trajectory; Figure 4c), and $\theta = 180°$ (downwind direction; Figure 4d). The latitudinal coordinate δ ($-90° \le \delta \le +90°$) describes directions out of the Earth orbit plane, while the longitudinal coordinate α ($0° \le \alpha \le 360°$) is measured from the downwind direction (Figure 4a). The maps show directions where interstellar helium atom fluxes come from. In other words, these are the directions where one would point an instrument to detected corresponding intensities. Bright dots in Figures 4c and 4d at $\delta = 0°$ show directions to the Sun.

[26] As expected, the directional intensity distribution at the upwind observation point ($\theta = 0°$) is axisymmetric and centered on the direction $\delta = 0°$ and $\alpha = 180°$ for the assumed interstellar wind velocity vector $\mathbf{V_0}$ in the plane of the Earth orbit. At the downwind observation point ($\theta = 180°$), interstellar helium fluxes form an axisymmetric annulus in the sky map.

[27] At $\theta = 126°$, the map shows two regions with the incoming interstellar helium flux. Interstellar helium atom intensities with direct trajectories peak in the direction tangential to the Earth orbit at $\alpha \approx 144°$; another peak corresponds to indirect trajectories at $\alpha \approx 270°$. The indirect He atom flux is significantly smaller because of much higher losses; the corresponding survival probabilities are 0.12 ($\theta^* = 360° - \theta = 234°$) and 0.51 ($\theta^* = \theta = 126°$) for indirect and direct trajectories, respectively. Directional spreads of interstellar helium fluxes are smaller in the Earth orbit plane than in the normal plane, with velocity variances sometimes described by corresponding effective "perpendicular" and "normal" temperatures. The asymmetry of local effective temperatures is caused by specifics of atom trajectories in the gravitational field [e.g., *Fahr*, 1968; *Wallis and Hassan*, 1978; *Gruntman*, 1980].

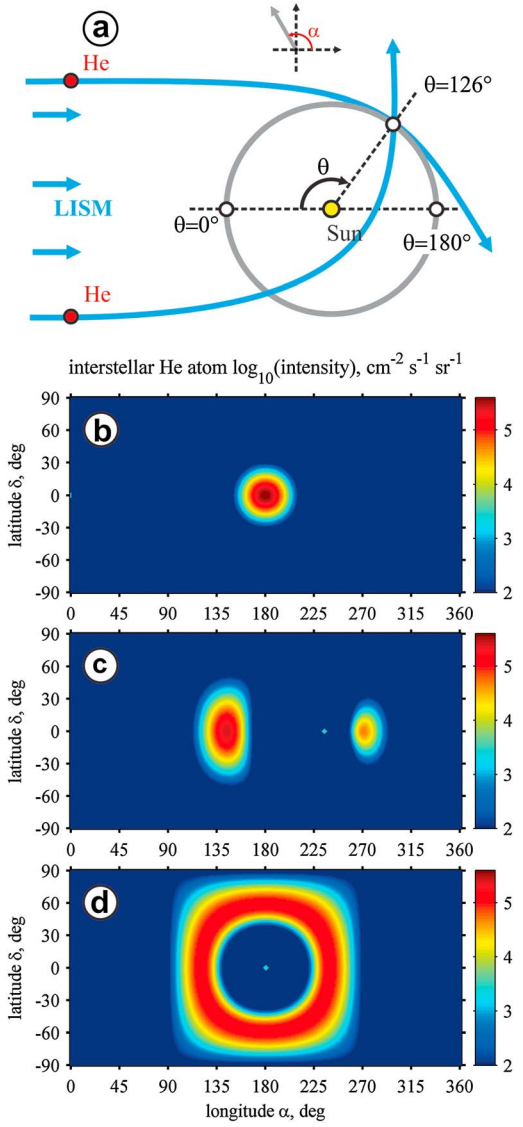

Figure 4. Interstellar He atom all-sky intensity (logarithmic scale) maps for observers (a) at rest at 1 AU at positions (b) $\theta = 0°$ (upwind), (c) $\theta = 126°$, and (d) $\theta = 180°$ (downwind) for the LSIM velocity $V_0 = 25$ km s^{-1}, temperature $T_0 = 8000$ K, and helium number density $n_0 = 0.01$ cm^{-3}. The longitudinal angle $\boldsymbol{\alpha}$ is counted from the downwind direction (Figure 4a); small bright dots (at latitude $\delta = 0°$) in Figures 4c and 4d show directions to the Sun.

3. Helium Atom Collisions With Solar Wind Protons

[28] An interstellar helium atom may experience elastic collisions with the solar wind ions on its trajectory from the LISM to a given point in the heliosphere. In this work, we consider only collisions with protons which establish a lower limit on collisional heating of interstellar helium and formation of the flux halo. While protons are most abundant ions in the solar wind, collisions with alpha-particles and perhaps even multiple-charged oxygen ions may lead to some additional helium atom intensities at large angles from the flux core. A quantitative evaluation of such collisions is beyond the scope of this work and will be done in the future.

[29] An elastic collision of a proton (mass m_1) with a helium atom (mass $m_2 = m_{\rm He}$) results in scattering of particles and change of their momenta and energies. A number of books, e.g., *Mott and Massey* [1949], *McDaniel* [1964], and *Landau and Lifshitz* [1976, 1977], detail fundamentals of scattering. Velocities of interstellar helium atoms do not exceed 100 km s^{-1} at heliocentric distances larger than 0.2 AU while solar wind velocities vary from 350 to 800 km s^{-1}. For such velocities, one can treat proton-helium elastic collisions as scattering in a spherically symmetric interaction potential field depending on the internuclear distance between colliding particles.

[30] Scattering can be conveniently described and calculated in a reference frame of the center of mass of colliding particles and then applied for obtaining post-collision particle velocities in a desired system of coordinates. Let us first consider scattering of a solar wind proton with a relative velocity V_r on an interstellar helium atom at rest in the heliocentric system (Figure 5). Scattering on an angle χ in the center-of-mass system would correspond to proton scattering on an angle θ_1 in the heliocentric reference frame (laboratory frame) such that

$$\tan\theta_1 = \frac{m_2 \sin\chi}{m_1 + m_2 \cos\chi}. \tag{6}$$

[31] For small scattering angles, the scattering angle in the laboratory frame θ_1 is approximately proportional to the angle χ. The helium atom would acquire a velocity $V_{He,2}$ in the collision,

$$V_{\rm He,2} = \frac{2m_1}{m_1 + m_2} \sin\left(\frac{\chi}{2}\right) V_r, \tag{7}$$

in the direction pointed at an angle

$$\theta_2 = \frac{\pi - \chi}{2} \tag{8}$$

with respect to the relative velocity vector $\mathbf{V_r}$. Because of axial symmetry, there is no dependence on the azimuthal scattering angle. For small scattering angles χ, the angle θ_2 is close to 90°.

[32] Figure 6 shows the dependence of the post-collision velocity $V_{\rm He,2}$ of the He atom (initially at rest) on the scattering angle χ for a relative collision velocity $V_r = 450$ km s^{-1}. Interstellar He atoms are not at rest in the heliosphere, however, but accelerate from $V_0 = 20 - 30$ km s^{-1} in the LISM up to about 50 km s^{-1} as they approach 1 AU. Scattering

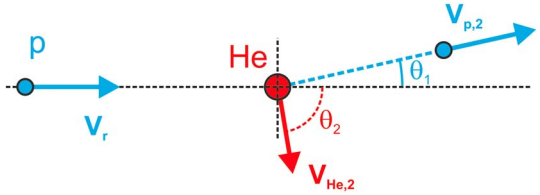

Figure 5. Collision of a proton with a relative velocity vector $\mathbf{V_r}$ with a He atom initially at rest; $\mathbf{V_{p,2}}$ and $\mathbf{V_{He,2}}$ are velocity vectors of the proton and the He atom, respectively, after the collision.

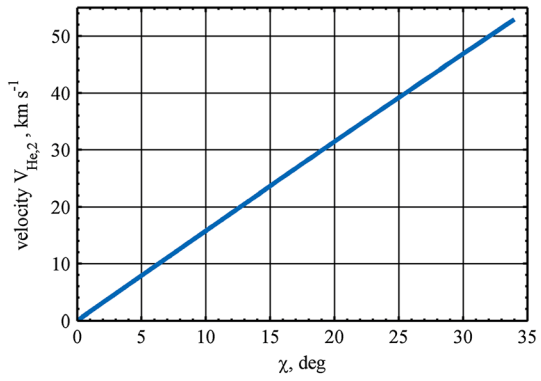

Figure 6. Dependence of the post-collision velocity $V_{He,2}$ of a He atom (initially at rest) on the scattering angle χ in the center-of-mass system for the relative collision velocity $V_r = 450$ km s^{-1}.

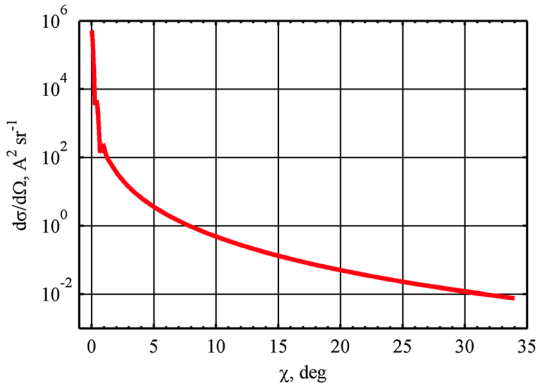

Figure 7. Differential scattering cross-section of protons on helium atoms as a function of the scattering angle χ in the center-of-mass reference frame for the relative collision velocity 450 km s^{-1}.

on angles χ larger than a few degrees corresponds to atom velocity increments $V_{\mathrm{He},2} > 5$ km s^{-1}, and such collisions would significantly change direction and magnitude of interstellar helium atom velocities and thus modify their velocity distributions and intensities.

[33] We calculated proton-helium differential elastic scattering [e.g., *Mott and Massey*, 1949; *McDaniel*, 1964; *Landau and Lifshitz*, 1976, 1977] using the analytical fit of *Helbig et al.* [1970] for the $(H^+)+(He)$ interaction potential of *Wolniewicz* [1965]. At scattering angles smaller than a few degrees, we treated scattering quantum mechanically (quasiclassically) with the Jeffreys-Wentzel-Kramers-Brillouin (JWKB) approximation for phase shifts. At angles larger than 1°, the classical treatment was applied. The quantum mechanical and classical cross-section curves were then patched in the region where they overlapped with identical dependences. *Johnson et al.* [1989] performed perhaps the most detailed experimental study of differential scattering of protons on helium in the 0.5–5.0 keV proton energy range (in the laboratory reference frame). We validated our calculations by direct comparison with the experimentally obtained differential cross-sections at relative collision velocities 538 km s^{-1} (proton energy 1500 eV in the laboratory frame) and 982 km s^{-1} (5000 eV).

[34] Figure 7 shows the calculated elastic differential scattering cross-section $d\sigma/d\Omega$ as a function of the scattering angle χ for the relative collision velocity 450 km s^{-1}. Quantum mechanical oscillations are prominent at small scattering angles and disappear at larger angles as expected. The classical and quantum mechanical calculations are patched at $\chi = 1.5°$. The total elastic scattering cross-section,

$$q_0 = \int \frac{d\sigma}{d\Omega} d\Omega = 2\pi \int_0^{\pi} \frac{d\sigma}{d\Omega}(\chi)\, d\chi, \qquad (9)$$

is 6.3×10^{-16} cm^2 (6.3 Å^2) at this collision velocity.

[35] At small collision impact parameters (corresponding to large scattering angles), non-elastic processes—charge exchange and proton impact ionization—become important and result in loss of helium atoms. Charge exchange dominates loss of helium atoms in collisions for typical solar wind velocities from 400 to 800 km s^{-1}. At $V_r = 450$ km s^{-1}, the charge exchange cross-section is 5×10^{-19} cm^{-2} [*Barnett et al.*, 1990].

[36] Let us make a simplifying assumption [*Gruntman*, 1986] that collisions are purely elastic at impact parameters b larger than a certain minimal impact parameter b_0 and result in helium atom loss for smaller impact parameters, $b < b_0$. Widely separated energy levels of the colliding particles and a large energy gap for charge exchange justifies such a simplification for proton-helium collisions. The particles exchange an electron at close encounters in contrast to symmetric collisions (e.g., between protons and hydrogen atoms) with no energy threshold and possible electron exchange at large internuclear distances.

[37] One can estimate the minimal impact parameter b_0 for elastic proton-helium collisions from

$$q_L = \pi b_0^2, \qquad (10)$$

where q_L is the loss process cross-section. We limit our calculations of differential scattering to impact parameters b $b_0 = 0.05$ Å which corresponds to the loss cross-section $q_L \approx 8 \times 10^{-19}$ cm^2, approximately what one expects for combined cross-sections contributing to helium atom losses in collisions with protons at a velocity 450 km s^{-1}. The limiting impact parameter $b_0 = 0.05$ Å corresponds to the maximum scattering angle $\chi_{\mathrm{MAX}} \approx 34°$ in the center-of-mass reference frame (Figures 6 and 7).

[38] In reality, atom loss could occur with some probability at impact parameters larger than b_0, $b > b_0$ (and $\chi < \chi_{\mathrm{MAX}}$), and some collisions with $b < b_0$ (and $\chi > \chi_{\mathrm{MAX}}$) would remain elastic. The simplifying assumption of a sharp impact parameter boundary between elastic and inelastic scattering results in (i) some excessive scattering on angles close to the maximum angle χ_{MAX}, say from 30°–34°, in the calculated differential cross-sections and (ii) some undercount of scattering on angles larger than 34°; the total elastic scattering cross-section q_0 remains unchanged. Since only a very small fraction of collisions leads to scattering on large angles, the introduced simplification would have practically no effect on the obtained results.

[39] In addition to the proton-helium total elastic scattering cross-section q_0 (for scattering on all angles, $\chi > 0°$), we also

introduce a partial cross-section, q_1, for scattering on angles larger than a certain minimal angle χ_1,

$$q_1 = 2\pi \int_{\chi_1}^{\pi} \frac{d\sigma}{d\Omega}(\chi)\, d\chi. \quad (11)$$

[40] For the minimal angle $\chi_1 = 1°$, the corresponding partial cross-section is $q_1 = 0.56$ Å^2 for the 450 km s^{-1} collision velocity. We explain below in this section the rationale for the introduction of this partial cross-section q_1.

[41] We assume henceforth a spherically symmetric solar wind flux expanding with the constant velocity $V_{SW} = 450.0$ km s^{-1} and the number density $n_{SW} = 5.0$ cm^{-3} at 1 AU. Then, the collision rate of helium atoms with the solar wind protons would be

$$\beta(R) = \beta_E \left(\frac{R_E}{R}\right)^2, \quad (12)$$

where

$$\beta_E = \beta(R_E) = n_{SW} V_{SW} q \quad (13)$$

is the collision rate at 1 AU for the corresponding collision cross-section q. Table 1 summarizes proton-helium collision rates $\beta_{E,0}$ and $\beta_{E,1}$ at 1 AU for the total and partial cross-sections q and q_1, respectively. (We consider all proton-helium collisions in the heliosphere occurring with the differential cross-section corresponding to the same relative collision velocity 450 km s^{-1}, as discussed below in section 4.)

[42] The average number of elastic collisions γ experienced by a helium atom on its way from infinity in the LISM to a point at a heliocentric distance R and an angle θ^* from the incoming asymptote of the hyperbolic orbit is an integral along the trajectory

$$\gamma = \int \beta(t)\, dt. \quad (14)$$

[43] Substituting integration over angle θ^* for that over time, one obtains

$$\gamma = \frac{\beta_E R_E^2}{h_0}\theta^*, \quad (15)$$

where $h_0 = h_0(R,\theta^*)$ is specific angular momentum of the atom.

[44] Figure 8 shows the dependence of the average numbers of elastic collisions γ_0 and γ_1 on the position angle θ at the Earth orbit for the cold model (or, generally, on the angle θ^* from the incoming asymptote) experienced by interstellar helium atoms on their trajectories from the LISM for the total cross-section q_0 and the partial cross-section q_1 (and the corresponding collision rates $\beta_{E,0}$ and $\beta_{E,1}$). Trajectories with large angles θ pass closer to the Sun and consequently experience larger numbers of collisions.

Table 1. Collision Rates $\beta_{E,0}$ and $\beta_{E,1}$ With Solar Wind Protons and Photo-Ionization Rate η_E for He Atoms at 1 AU

Process	Angle	Cross-section	Rate at 1 AU
Elastic scattering	$\chi > 0°$	$q_0 = 6.31$ Å^2	$\beta_{E,0} = 1.42 \times 10^{-7}$ s^{-1}
Elastic scattering	$\chi > 1°$	$q_1 = 0.56$ Å^2	$\beta_{E,1} = 1.27 \times 10^{-8}$ s^{-1}
Photo-ionization			$\eta_E = 1.0 \times 10^{-7}$ s^{-1}

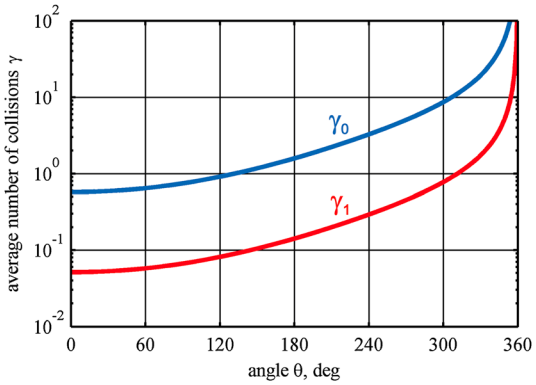

Figure 8. Average numbers of collisions γ_0 and γ_1 for elastic scattering on angles $\chi > 0°$ and $\chi > 1°$ (with the corresponding rates $\beta_{E,0}$ and $\beta_{E,1}$, respectively, at 1 AU from the Sun) as a function of the position angle θ at the Earth orbit for the cold model (or, generally, of the angle θ^* from the incoming asymptote).

[45] For collisions on all angles ($\chi > 0$), the average collision number γ_0 is close to one at most interesting for experiments position angles where interstellar helium trajectories reach the Earth orbit tangentially, $\gamma_0 = 0.95$ at $\theta = 126°$. The Poisson distribution describes probabilities of helium atoms to experience a certain number of collisions. For example, for the average number of collisions $\gamma_0 = 1.0$, a significant fraction of atoms would experience more than one collisions—the probabilities of 0, 1, and more than 1 collision would be 37%, 37%, and 26%, respectively.

[46] Direct calculations of helium atom trajectories with multiple elastic collisions pose major difficulties. One can however simplify the problem if helium atoms experience either only one elastic collision or no collisions at all. Such a "one-or-none collision" approximation could be justified if the average number of collisions is significantly smaller than one, that is for $\gamma \ll 1$, which is clearly not the case for collisions with the total cross-section q_0.

[47] Most scattering in proton-helium collisions occurs on small angles (Figure 7), and such collisions would add very small velocity increments to He atoms (Figure 6) and thus contribute very little to broadening of the flux of helium atoms [*Gruntman*, 1986]. Therefore, one can disregard scattering on small angles and consider only collisions with scattering on angles larger than a certain limiting minimum angle χ_1. Typical velocities $V_{He,2}$ imparted to helium atoms in such small angle collisions would determine the disregarded directional change (let us call it the angle ψ) of atom trajectories. The number of such small angle collisions experienced by a He atom approximately equals the calculated average number of collisions γ_0, and it is thus ~1 for direct trajectories (Figure 8). Therefore, the calculated shape of He atom directional intensity distributions with disregarded small angle collisions would be accurate roughly within the angle ψ for direct trajectories and perhaps twice as large for indirect trajectories with larger number of collisions.

[48] Let us choose a convenient limiting minimum scattering angle $\chi_1 = 1°$. Then, considering only scattering on angles $\chi > \chi_1$ with the introduced earlier corresponding partial cross-section q_1, the average number of collisions γ_1 would not exceed 0.10 for direct trajectories crossing the Earth orbit at $\theta < 145°$, including in the region of most interest for experiments (Figure 8). For $\gamma_1 = 0.10$, the fraction of atoms experiencing more than one collision is about 1/20 of the particles with one collision. Therefore, atoms with multiple collisions can be disregarded without introducing a significant error in the calculations of the collision-formed flux halo. The average number of collisions with $\chi > \chi_1$ would be only $\gamma_1 = 0.142$ at $\theta = 180°$ and reach $\gamma_1 = 1.0$ at a very large position angle $\theta = 311°$. Indirect trajectories to the observation point with the position angle $\theta = 126°$ would be characterized by the angle $\theta^* = 360° - \theta = 234°$ with the average number of collisions $\gamma_1 = 0.27$, making the one-or-none collision approximation still applicable. To summarize, under the one-or-none collision approximation, we will assume that for the average number of collisions γ_1, a γ_1 fraction of He atoms would experience one collision and the remaining $(1 - \gamma_1)$ fraction would experience no collisions.

[49] Proton-helium scattering on angles χ equal to 1° and 0.3° corresponds to velocity increments $V_{He,2}$ imparted to He atoms 1.6 and 0.5 km s^{-1}, respectively (Figure 6). For the latter velocity increment, the angle ψ characterizing changes of He atom velocity directions would not exceed 1°. In fact, this angle would be smaller since only a component of the imparted velocity $V_{He,2}$ which is perpendicular to the local He atom velocity vector causes the change in its direction. We note that only 20% of atoms that experience a collision would scatter on angles $\chi > 0.3°$. Therefore, we can conservatively estimate that, for the selected minimal angle $\chi_1 = 1°$, the accuracy of the calculations of the shape of He atom directional intensity distributions under the one-or-none collision approximation would not be worse than $\psi \le 1°$.

4. Interstellar He Atom Halo Fluxes at 1 AU

[50] Elastic collisions of interstellar helium with solar wind protons result in two effects [*Gruntman*, 1986]. First, the flux core intensity is slightly diminished because of scattering of some atoms on large angles from the core. Second, the scattered atoms form the flux halo. We adopt in this work the one-or-none collision approximation with the limiting minimal scattering angle $\chi_1 = 1°$. Consequently, the halo intensities would be accurately calculated at angles larger than 1° from the flux core ($\psi \le 1°$).

[51] Let us consider He atoms reaching an arbitrary point $\mathbf{R} = (R,\theta)$ with a velocity $\mathbf{V}$ with respect to the Sun. Figure 9 shows trajectories of such particles for the conventional model without collisions (top) and for the model with one elastic collision (bottom). The trajectories and the collisions are considered in a general three-dimensional case. The plane of the figure (top and bottom) contains the ecliptic plane and the radius-vector $\mathbf{R}$. We assume that the interstellar wind velocity vector $\mathbf{V_0}$ is in the ecliptic plane and points in the direction of the x axis. (The gray circle represents the Earth orbit if $R = R_E$.) The velocity vectors $\mathbf{V_1}$, $\mathbf{V_2}$, $\mathbf{V_3}$, $\mathbf{V_4}$, $\Delta\mathbf{V}$, and the radius-vector $\mathbf{R_1}$ are not necessarily in the plane of the figure.

[52] In both cases with and without collisions, we begin with atoms with the same velocity $\mathbf{V}$ at the same selected point $\mathbf{R}$ and trace them back to the LISM where they would have velocities $\mathbf{V_1}$ (Figure 9, top) and $\mathbf{V_2}$ (Figure 9, bottom), respectively. In the case without collisions, as described in section 2, we first determine the velocity $\mathbf{V_1}$ and the angle θ^* between the incoming radial asymptote of the hyperbola and the radius-vector $\mathbf{R}$. Then, we calculate the survival probability to reach the selected point and obtain the local velocity distribution function. Finally, we numerically integrate the velocity distribution over velocity magnitudes in a selected direction to obtain the He atom intensity from that direction.

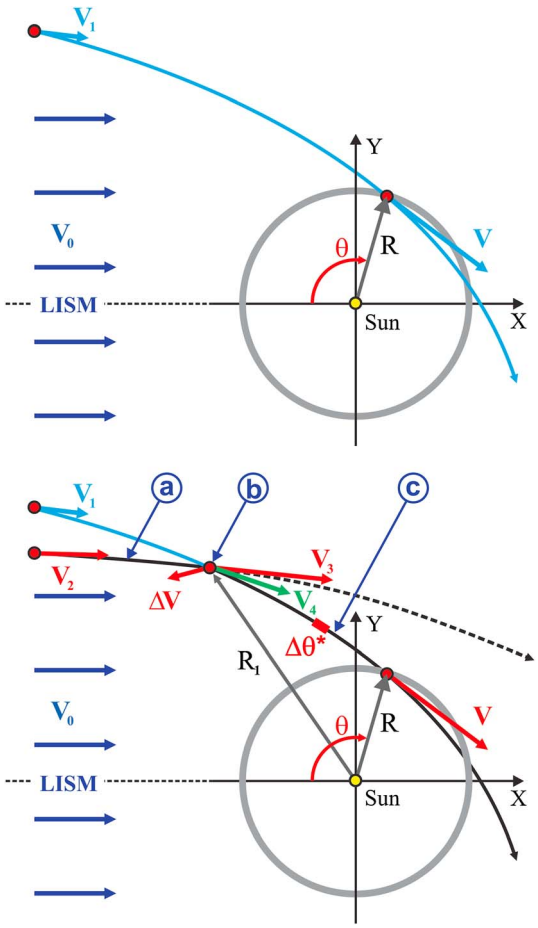

Figure 9. Trajectories of interstellar He atoms originating in the LISM with the initial velocities $\mathbf{V_1}$ and $\mathbf{V_2}$ and reaching the same point $\mathbf{R} = (R,\theta)$ with the same velocity $\mathbf{V}$ without collisions (top) and with one elastic collision at the point $\mathbf{R_1}$ (bottom), respectively. Please see the text for explanations of velocity vectors $\mathbf{V_3}$, $\mathbf{V_4}$, and $\Delta\mathbf{V}$ and trajectory segments (a), (b), and (c) in the bottom panel.

[53] In the one-or-none collision case, we also first determine—for the given $\mathbf{V}$ and $\mathbf{R}$—the orbital parameters of the trajectory, then calculate the fraction of atoms that does not experience collisions and obtain their contribution to the intensity as described above. Consider now an interstellar atom originating in the LISM with the velocity vector $\mathbf{V_2}$ and reaching the point $\mathbf{R}$ with the velocity $\mathbf{V}$ and experiencing one elastic collision at the point $\mathbf{R_1}$. Let us divide the atom trajectory into three segments (a), (b), and (c) (Figure 9, bottom). In segment (a), the atom starts from the LISM with the (unknown and to be determined) velocity

$\mathbf{V_2}$ and reaches the collision point $\mathbf{R_1}$ with a velocity $\mathbf{V_3}$. Then in segment (b), the atom experiences an elastic collision at this point and acquires a velocity increment $\mathbf{\Delta V}$ such that its post-collision velocity vector is $\mathbf{V_4} = \mathbf{V_3} + \mathbf{\Delta V}$. Finally in segment (c), the atom starts from the point $\mathbf{R_1}$ with the initial velocity $\mathbf{V_4}$ and reaches the point $\mathbf{R}$ with the velocity $\mathbf{V}$.

[54] To trace this He atom from the selected point $\mathbf{R}$ back to the LISM, we begin with segment (c) of the trajectory. The collision may occur at different points along the trajectory, so we integrate along the trajectory the contributions of such events to the intensity. Therefore, we divide the hyperbolic orbit into equal intervals $\Delta\theta^*$ of the angle between the incoming radial asymptote and the radius-vector $\mathbf{R}$. Consider a collision at a point $\mathbf{R_1}$. Here, the probability Δp of a collisions in the angular interval $\Delta\theta^*$ is independent of the angle from the asymptote and equals

$$\Delta p = \frac{\beta_{E,1} R_E^2}{h_c} \Delta\theta*, \tag{16}$$

where h_c is specific angular momentum of the He atom in segment (c) of the trajectory (Figure 9, bottom). Then, we obtain (from the trajectory orbital elements) the velocity $\mathbf{V_4}$ at the point $\mathbf{R_1}$ which is the velocity of the He atom after the elastic collision at this point. Accounting for atom losses on segment (c) of the trajectory, we relate the post-collision phase space density of atoms at the point $\mathbf{R_1}$ and the phase space density at the point $\mathbf{R}$.

[55] Similarly in segment (a) of the trajectory, we relate the atom phase space density at the point $\mathbf{R_1}$ with the velocity $\mathbf{V_3}$ before the collision and the atom phase space density with the velocity $\mathbf{V_2}$ in the Maxwellian distribution at infinity in the LISM. The velocity $\mathbf{V_2}$ and atom losses on this segment are calculated from the trajectory orbital elements, obtained from $\mathbf{V_3}$ and $\mathbf{R_1}$.

[56] At the collision point $\mathbf{R_1}$, the pre-collision velocities of the solar wind proton $\mathbf{V_{p,1}}$ and the interstellar He atom $\mathbf{V_3}$ change to the post-collision velocities $\mathbf{V_{p,2}}$ and $\mathbf{V_4}$, respectively,

$$(\mathbf{V_{p,1}}, \mathbf{V_3}) \Rightarrow (\mathbf{V_{p,2}}, \mathbf{V_4}), \tag{17}$$

with the relations between velocities determined by conservation of momentum and energy for given scattering angles. The differential cross-section $\frac{d\sigma}{d\Omega}(\chi, \varphi)$ (Figure 7) describes the probability to scatter (in the center-of-mass reference frame) on an angle χ, with the azimuthal angle φ distributed uniformly. The angle χ also determines the magnitude of the velocity increment ΔV of the He atom in the collision.

[57] Typical velocities of interstellar helium atoms at $R > 1$ AU are 20–50 km s^{-1} while the velocity of solar wind protons is 450 km s^{-1}. The magnitude of relative collision velocities would thus vary less than 10%, depending on the collision place and relative orientations of these two velocity vectors. We disregard the dependence of the differential cross-section on the relative collision velocity and assume that all collisions are characterized by the differential cross-section corresponding to the same effective velocity 450 km s^{-1}. The realistic solar wind velocity continuously changes with time. These temporal variations would average out differential cross-section dependences over a range of collision velocities, thus justifying the assumption of a differential cross-section at one effective velocity. (The He atom collision cross-sections and corresponding rates, equation (13) and Table 1, are also obtained for this collision velocity of 450 km s^{-1}, consistent with the assumption above.)

[58] One cannot make, however, a similar simplifying assumption about the radial direction of relative collision velocities. For typical velocities of colliding particles, relative collision velocities could deviate from the radial direction by as much as 6°. Many elastic collisions result in scattering smaller than this angle. Consequently, the assumption of the radial relative collision velocity would have resulted in similar, up to 6°, and thus unacceptable errors in determining He atom trajectories.

[59] If the heliocentric velocities of both particles were known either before or after the collision, then calculating unknown velocities would have been straightforward. One would have first to determine the velocity vector of the center of mass of the colliding particles; then calculate changes in particle velocities in the center-of-mass system for given scattering angles χ and φ, and finally obtain the unknown velocities in the reference system at rest with respect to the Sun.

[60] At the collision point $\mathbf{R_1}$, we know one pre-collision velocity ($\mathbf{V_{p,1}}$) and one post-collision velocity ($\mathbf{V_4}$) of the colliding particles (equation (17)) and the two other velocities, $\mathbf{V_{p,2}}$ and $\mathbf{V_3}$, are unknown. We numerically solve the equations relating these four velocities for given scattering angles χ and φ in the center-of-mass system and obtain the velocity $\mathbf{V_3}$ of the He atom before the collision in the heliocentric system. Conservation of atoms in collisions allows us then to relate the phase space densities of He atoms before and after the collision. Patching the relations between atom velocities and phase space densities in segments (a), (b), and (c) of the entire trajectory, we relate the phase space density of interstellar He atoms reaching the point $\mathbf{R}$ with the given velocity $\mathbf{V}$ and experiencing one elastic collision at the point $\mathbf{R_1}$ with the phase space density of atoms with velocity $\mathbf{V_2}$ in the LISM.

[61] The calculations of the He atom intensity at a given point from a given direction thus requires quadruple integration over (i) atom velocity magnitudes V; (ii) along atom trajectory (angle θ^*) for the given V, with equation (16) describing local contributions (probabilities) of collisions along the trajectory; and (iii and iv) over scattering angles χ and φ describing the differential cross-section. In this work, we directly integrate over the velocity V and along the trajectory over the angle θ^* and use the Monte Carlo technique to evaluate the double integral over scattering angles χ and φ.

[62] Figure 10 shows angular distributions in longitude ("cuts" of all-sky maps at latitude $\delta = 0°$) of interstellar He atom intensities for the conventional model without collisions (solid blue lines), due to collisions only (solid green line), and for one-or-none collision approximation adopted in this work (red dotted lines) for position angles $\theta = 0°$ (top), $\theta = 126°$(middle), and $\theta = 180°$ (bottom) for an observer at rest at 1 AU from the Sun. The longitudinal angle α is measured from the downwind direction (Figure 4a). The intensity distributions are "cuts" (slices), in the plane of Figure 4a, of the all-sky maps in Figures 4b–4d. The red dotted lines represent the "real" interstellar helium atom intensities accounting for elastic collisions in contrast to the

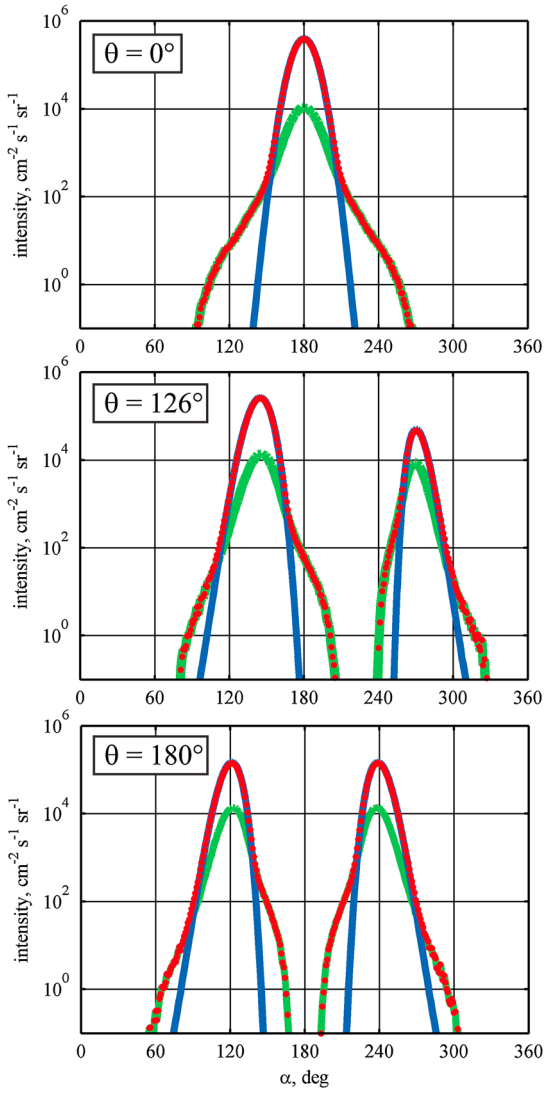

Figure 10. Longitudinal angular distributions of interstellar He atom intensities for the conventional model without collisions (solid blue lines), due to collisions only (solid green), and for the one-or-none collision approximation adopted in this work (red dotted lines) for position angles $\theta = 0°$ (top), $\theta = 126°$ (middle), and $\theta = 180°$ (bottom) for an observer at rest at 1 AU from the Sun. The distributions correspond to the "cuts" (at latitude $\delta = 0°$) of the full sky maps (without collisions) shown in Figures 4b–4d.

solid blue lines showing intensities obtained by the conventional model without collisions.

[63] One can see that the collisions practically do not change the flux core but produce the flux halo, confirming earlier predictions by *Gruntman* [1986]. For the upwind direction ($\theta = 0°$), the collisions form "shoulders" of intensity distributions approximately 30° wider than the flux core without collisions. The shoulder intensities are three to four orders magnitude smaller than the peak intensity of He atoms. At still larger angles from the core, the collision-produced intensities drop precipitously.

[64] In the downwind direction ($\theta = 180°$), the interstellar He flux core forms an annulus in the sky map (Figure 4d). The interstellar He atoms that experienced a collision partially fill the directions within this annulus (Figure 10, bottom) and show the halo outside. The angle $\alpha = 180°$ corresponds to the direction to the Sun. Consequently, interstellar He atoms pass close to the Sun with significant loss, explaining steep intensity drop near $\alpha = 180°$. The distributions at $\theta = 126°$ clearly show the difference in intensities between direct atom trajectories at $\alpha \approx 144°$ and indirect trajectories at $\alpha \approx 270°$. The collision-produced He atom halo is relatively much more pronounced for indirect trajectories, as expected, passing closer to the Sun with higher probabilities of collisions.

[65] Let us now consider, as an example, interstellar helium intensities seen by an observer moving with the Earth. Figure 11 (bottom) shows a calculated full sky map of interstellar helium intensities in the ecliptic coordinates for a realistic direction of the interstellar wind (ecliptic latitude −5° and longitude 75°). The observer is at the point with ecliptic longitude $\lambda = 129°$, which corresponds to the

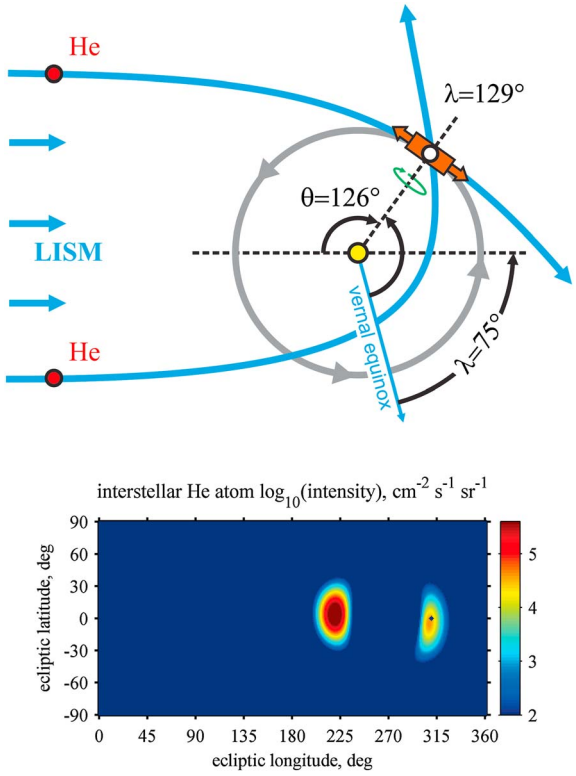

Figure 11. Interstellar He atom all-sky intensity (logarithmic scale) map in ecliptic coordinates (bottom) for an observer moving with the Earth (top) at the point with ecliptic longitude $\lambda = 129°$, corresponding to the position angle $\theta = 126°$ measured from the projection (dashed horizontal line) of the upwind (interstellar wind) direction on the ecliptic plane for the LSIM velocity $V_0 = 25$ km s^{-1}, temperature $T_0 = 8000$ K, and helium number density $n_0 = 0.01$ cm^{-3}; the interstellar wind velocity vector points in the direction with ecliptic latitude $\beta = -5°$ and ecliptic longitude $\lambda_{ISW} = 75°$. Direct and indirect trajectory intensities peak in directions at ecliptic longitudes 220° and 308°, respectively (bottom). The dark dot at ecliptic latitude 0° near the center of the indirect peak shows the direction to the Sun. The top panel also shows spinning of a sun-pointed spacecraft with instruments (arrows) pointed normal to the spin axis.

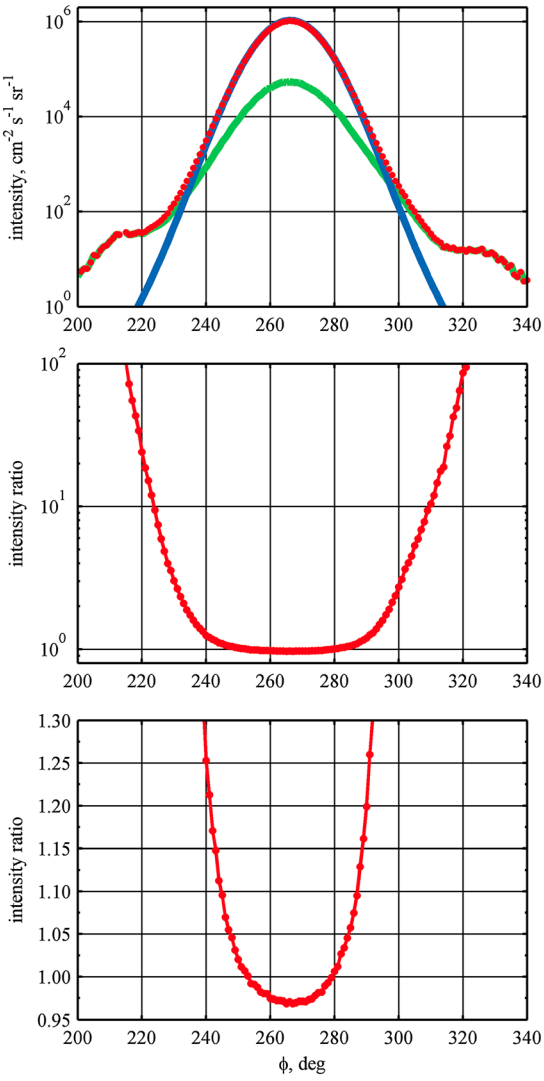

Figure 12. The top panel shows interstellar He atom intensities (swath in the sky) in the plane normal to the direction toward the Sun as a function of the pointing angle ϕ counted from the southern ecliptic pole at a point with ecliptic longitude $\lambda = 129°$, corresponding to the position angle $\theta = 126°$ (Figure 11), for the conventional model without collisions (solid blue line); due to collisions only (solid green); and for the one-or-none collision approximation adopted in this work (red dotted line) for an observer moving with the Earth. The ratios of the intensities for the model with collisions to those for the conventional model without collisions are shown in the bottom (linear scale) and top (logarithmic scale) panels.

position angle $\theta = 126°$ from the projection of the upwind direction on the ecliptic plane. Direct trajectories tangentially touch the circular Earth orbit at this point (Figure 11, top). Similarly to Figure 4, the map shows directions from where interstellar helium atom fluxes come. Direct and indirect flux intensities peak in directions at ecliptic longitudes 220° and 308°, respectively, and they are shifted by about 5° above and below the ecliptic plane. The dark dot with ecliptic latitude 0° and longitude 309° near the center of the indirect peak shows the direction to the Sun.

[66] Figure 11 (top) also illustrates observational geometry for obtaining all-sky maps from a spinning spacecraft with the spin axis pointed at the Sun [e.g., *Gruntman et al*., 2001]. The instruments pointing in the direction normal to the spin axis image the swath in the sky. As the spacecraft revolves around the Sun in a heliocentric orbit (e.g., an Earth-bound spacecraft), its Sun-pointed spin axis follows the Sun, and the normally pointed instruments achieve the coverage of the entire sky twice during one complete orbit. The Earth-bound IBEX spacecraft operates in such a mode [*McComas et al*., 2009], at any given moment measuring interstellar He fluxes in a swath of the sky [*Moebius et al*., 2009a,2009b] determined by pointing of the spacecraft spin axis (Figure 11, top).

[67] Figure 12 (top) shows, as an example, the calculated He atom intensities in such a swath in the sky at the observation point with ecliptic longitude $\lambda = 129°$ ($\theta = 126°$) for the conventional model without collisions (solid blue lines) and for the one-or-none collision approximation (red dotted line) for an observer moving with the Earth. The curves are cuts through the intensity map, shown in Figure 11 (bottom), in the plane normal to the direction to the Sun. The pointing direction (angle ϕ) is measured from the ecliptic South Pole as the observing platform spins in the clockwise direction about the vector pointed at the Sun. Therefore, the angle $\phi = 270°$ would correspond to the direction tangential to the Earth orbit in the ecliptic plane and pointed in the direction of the Earth motion. This is a general direction from where the incoming interstellar He atoms would have the highest velocities relative to the moving Earth, which is most favorable for observations.

[68] The middle and bottom panels of Figure 12 show the ratios of intensities obtained by the model with collisions, introduced in this work, to those obtained by the conventional model of interstellar helium without collisions. One can see that proton-helium elastic collisions reduce the maximum (peak) intensity by 3% and increase intensities in the wings of the distributions. This increase is about 25% at the angle of 25° from the peak intensity and it rapidly grows with the angle. In the flux halo, for example, the ratio of intensities is about a factor of 25 at the angle 45° from the maximum.

5. Conclusions

[69] The quantitative evaluation of the effect of elastic collisions, predicted more than 25 years ago, confirms the formation of the interstellar helium atom flux halo that could be measured at 1 AU. For an especially important point for observations near the ecliptic longitude $\lambda = 129°$, increased helium atom intensities are pronounced in the directions pointing away from the ecliptic plane, which makes it convenient for comparison with experimental data obtained from Sun-pointed spinning spacecraft.

[70] Let us summarize now the main simplifying assumptions made in this work and evaluate their potential effect on accuracy of the obtained results:

[71] (a) disregarding collisions with the solar wind heavier ions, particularly alpha particles;

[72] (b) considering only proton-helium scattering on angles larger than a certain minimum value, assumed in this work $\chi > 1°$ in the center-of-mass system;

[73] (c) sharp-impact parameter boundary between elastic and inelastic proton-helium collisions, assumed in this work $b_0 = 0.05$ Å;

[74] (d) one-or-none collision approximation (rather than a Poissonian distribution) for the number of collisions experienced by interstellar He atoms;

[75] (e) use of the differential cross-section calculated at a certain relative collision velocity, assumed in this work 450 km s^{-1};

[76] (f) disregarding anisotropy and deviations from the R^{-2} atom loss rate dependence on the heliocentric distance; and

[77] (g) considering helium atoms in hyperbolic trajectories only in segment (c) (Figure 9, bottom) and disregarding atoms in elliptical orbits.

[78] Only assumption (a) may lead to non-negligible underestimate of enhanced large-angle wings of directional He atom intensity distributions. Consequently, the interstellar helium atom flux halo, obtained in this work, is the lower limit on wing intensities. We will quantitatively examine the contributions of collisions with solar wind alpha-particles and multiple-charged ions in the future. Other assumptions could only marginally affect the accuracy of the obtained halo properties.

[79] Assumption (b) limits accuracy of intensity directional distributions within 1° of the flux core and thus has practically no effect on the halo. Assumptions (c) and (d) may only affect far wings, >50° from the maximum intensity peak, where intensities are far below realistic possibilities of direct detection. Assumption (e) would have practically no effect on properties of the halo because of the varying solar wind. Assumption (f) could lead to a slight overestimate only of He atom intensities in indirect trajectories. Uncertainties in knowledge of details of loss processes require use of an effective loss rate in any event. In addition, direct trajectories are of most interest for experiments so uncertainties of electron impact ionization, affecting primarily indirect trajectories, are of minor importance.

[80] Finally, assumption (g) disregards He atoms in elliptic trajectories arriving at observation points. Such atoms enter the solar system on hyperbolic trajectories from the LISM and elastic collisions with solar wind protons change their trajectories into elliptic orbits. Examination of velocity distributions of atoms arriving at an observational point at 1 AU from a given direction shows that atom velocities peak at magnitudes substantially larger than the minimal hyperbolic velocity (equal to the maximum elliptic orbit velocity) at this point. Therefore, contributions to intensity by such particles would be minimal.

[81] The lower limit on the wing intensities, obtained in this work, is a first step in a quantitative evaluation of the He atom flux halo caused by elastic collisions with solar wind ions and their possible comparison with directional distributions of interstellar helium flux intensities measured by IBEX [*Moebius et al*., 2009a, 2012; *Bzowski et al*., 2012]. In addition, accurate prediction of collisional heating and formation of the halo is essential and indispensable for probing possible deviations from Maxwellian velocity distributions of interstellar neutral atoms in the LISM.

[82] **Acknowledgment.** This work is supported, in part, by NASA's IBEX program.

References

Ajello, J. M., W. R. Pryor , C. A. Barth, C. W. Hord , A. I. F. Stewart, K. E. Simmons, and D.T. Ha1l (1994), Observations of interplanetary Lyman-α with the Galileo Ultraviolet Spectrometer: Multiple scattering effects at solar maximum, *Astron. Astrophys.*, *289*, 283–303.

Axford, W. I. (1972), The interaction of the solar wind with the interstellar medium, *Solar Wind, NASA SP-308*, 609–660.

Banaszkiewicz M., H. Rosenbauer, and M. Witte (1990), An inverse method of determination of the interstellar neutral gas distribution function, in *Physics of the Outer Heliosphere*, Proc. of 1st COSPAR Colloquium, pp. 359–362.

Banaszkiewicz, M., M. Witte and H. Rosenbauer (1996), Determination of interstellar helium parameters from the ULYSSES–NEUTRAL GAS experiment: Method of data analysis, *Astron. Astrophys. Suppl. Ser.*, *120*, 587–602.

Barnett, C. F., H. T. Hunter and M. I. Kirkpatrick, I. Alvarez, C. Cisneros, and R. A. Phaneuf (1990), *Atomic Data, for Fusio*n. Vol. 1. Collisions of H, H_2, He and Li atoms and ions with atoms and molecules, ORNL-6086/V1, Oak Ridge National Laboratory, Oak Ridge, Tennessee.

Battin, R. H. (1987), An Introduction to the Mathematics and Methods of Astrodynamics, AIAA, New York, New York.

Bertaux, J.-L. (1984), Helium and hydrogen of the local interstellar medium observed in the vicinity of the Sun, *IAU Colloquium No.81*, *NASA CP 2345*, 3–23.

Blum, P. W., J. Pfleiderer, and C. Wulf-Mathies (1975), Neutral gases of interstellar origin in interplanetary space, *Planet. Space Sci.*, *23*, 93–105; doi:10.1016/0032-0633(75)90070-7.

Brandt, J. C. (1964), Interplanetary gas. IX. Effects of the local interstellar medium, *Icarus*, *3*, 253–263; doi:10.1016/0019-1035(64)90021-1.

Bzowski, M.,et al. (2012), Neutral interstellar helium parameters based on IBEX-Lo observations and test particle calculations, *Astroph. J., Suppl. Ser.*, *198*(2), article id. 12; doi:10.1088/0067-0049/198/2/12.

Chassefiere, E., J. L. Bertaux, and V. Sidis (1986), Elastic collisions of solar wind protons with interstellar neutrals (H and He) inside the heliosphere: A new approach, *Astron. Astrophys.*, *169*, 298–304.

Danby, J. M. A. and G. L. Camm (1957), Statistical dynamics and accretion, *Mon. Not. Roy. Astron. Soc.*, *117*, 50–71.

Danby, J. M. A. and T. A. Bray (1967), Density of interstellar matter near a star, *Astronom. J.*, *72*, 219–222; doi:10.1086/110221.

Fahr, H. J. (1968), On the influence of neutral interstellar matter on the upper atmosphere, *Astrophys. Space Sci.*, *2*, 474–495; doi:10.1007/BF02175923.

Fahr, H. J. (1971), The interplanetary hydrogen cone and its solar cycle variations, *Astron. Astrophys.*, *14*, 263–275.

Fahr, H. J. (1974), The extraterrestrial UV-background and the nearby interstellar medium, *Space Sci. Rev.*, *15*, 483–540, doi:10.1007/BF00178217.

Fahr, H. J. (1978), Change of interstellar gas parameters in stellar-wind-dominated astrospheres: Solar case, *Astron. Astrophys.*, *66*, 103–117.

Fahr, H. J. (1979), Interstellar hydrogen subject to a net repulsive solar force field, *Astron. Astrophys.*, *77*, 101–109.

Fahr, H. J. and G. Lay (1974), Solar radiation asymmetries and heliospheric gas heating influencing extraterrestrial UV data, *Space Res.*, *14*, 567–573.

Fahr, H. J., D. Rucinski, and H. U. Nass (1987), Modeling of the interplanetary helium EUV-resonance glow for time-dependent solar radiation conditions, *Ann. Geophysicae*, *5*, 255–264.

Goldstein, H. (1980), Classical Mechanics, Addison-Wesley Publ. Co., Reading, Mass.

Gruntman, M. (1980), Interstellar helium at Earth orbit, *Preprint 543, Space Research Institute (IKI)*, USSR Academy of Sciences, Moscow.

Gruntman, M. (1986), Concerning the problem of collisional heating of the interstellar helium by solar wind protons, *Planet. Space Sci.*, *34*, 387–389; doi:10.1016/0032-0633(86)90145-5.

Gruntman, M. (1993), A new technique for in situ measurement of the composition of interstellar gas in the heliosphere, *Planet. Space Sci.*, *41*, 307–319; doi:10.1016/0032-0633(93)90026-X.

Gruntman, M. (1997), Energetic neutral atom imaging of space plasmas, *Rev. Sci. Instrum.*, *68*, 3617–3656; doi:10.1063/1.1148389.

Gruntman, M., E. C. Roelof, D. G. Mitchell, H. J. Fahr, H. O. Funsten, and D. J. McComas (2001), Energetic neutral atom imaging of the heliospheric boundary region, *J. Geophys. Res.*, *106*, 15767–15781; doi:10.1029/2000JA000328.

Hall, D., D. E. Shemansky, P. Gangopadhyay, M. Gruntman, and D. L. Judge (1993), Heliospheric hydrogen beyond 15 AU: Evidence for a termination shock, *J. Geophys. Res.*, *98*, 15185–15192; doi: 10.1029/93JA01175.

Helbig, H. F., D. B. Millis, and L. W. Todd (1970), Semiclassical calculation of elastic H^+−He differential scattering cross-sections, *Phys. Rev. A*, *2*, 771–774; doi:10.1103/PhysRevA.2.771.

Holzer, T. E. (1977), Neutral hydrogen in interplanetary space, *Rev. Geophys. Space Phys.*, *15*, 467–490; doi:10.1029/RG015i004p00467.

Johnson, L. K., R. S. Gao, R. G. Dixson, K. A. Smith, N. F. Lane, and R. F. Stebbings (1989), Absolute differential cross-sections for small-angle H^+−He direct and charge-transfer scattering at keV energies, *Phys. Rev. A*, *40*, 3626–3631; doi:10.1103/PhysRevA.40.3626.

Katushkina O. A., and V. V. Izmodenov (2011), Spectral properties of backscattered solar Ly-a radiation in the heliosphere: A search for heliospheric boundary effects, *Adv. Space Res.*, *48*, 1967–1979; doi:10.1016/j.asr.2011.08.026.

Lallement, R., J. L. Bertaux, and F. Dalaudier (1985), Interplanetary Lyman α spectral profiles and intensities for both repulsive and attractive solar force fields: Predicted absorption pattern by a hydrogen cell, *Astron. Astrophys.*, *150*, 21–32.

Landau, L. D., and E. M. Lifshitz (1976), *Mechanics, Course of Theoretical Physics*, vol. 1, 3rd ed., Pergamon Press.

Landau, L. D., and E. M. Lifshitz (1977), Quantum Mechanics. Non-Relativistic Theory. Course of Theoretical Physics, Volume 3, 3rd edn, Pergamon Press, New York.

Lee M. A., H. Kucharek, E. Mobius, X. Wu, M. Bzowski, and D. McComas (2012), An analytical model of interstellar gas in the heliosphere tailored to Interstellar Boundary Explorer observations, *Ap. J. Suppl.*, *198*, 10, doi:10.1088/0067-0049/198/2/10.

McComas, D. J., et al. (2009), IBEX—Interstellar Boundary Explorer, *Space Sci. Rev.*, *146*, 11–33; doi: 10.1007/s11214-009-9499-4.

McDaniel, E. W. (1964), Collision Phenomena in Ionized Gases, John Wiley and Sons, New York.

McMullin, D. R., et al. (2004), Coordinated observation of local interstellar helium in the Heliosphere. Heliospheric conditions that affect the interstellar gas inside the heliosphere, *Astron. Astrophys.*, *426*, 885–895, doi: 10.1051/0004-6361:20047147.

Meier, R. R. (1977), Some optical and kinetic properties of the nearby interstellar gas, *Astron. Astrophys.*, *55*, 211–219.

Mott, N. F., and H. S. W. Massey (1949), The Theory of Atomic Collisions, Oxford.

Moebius, E., et al. (2004), Coordinated observation of local interstellar helium in the heliosphere. Synopsis of the interstellar He parameters from combined neutral gas, pickup ion and UV scattering observations and related consequences, *Astron. Astrophys.*, *426*, 897–907; doi: 10.1051/0004-6361:20035834.

Moebius, E., et al. (2009a), Direct observations of interstellar H, He, and O by the Interstellar Boundary Explorer, *Science*, *236*, 969–971, doi: 10.1126/science.1180971.

Moebius, E., et al. (2009b), Diagnosing the neutral interstellar gas flow at 1 AU with IBEX-Lo, *Space Sci. Rev.*, *146*, 149–172; doi: 10.1007/s11214-009-9498-5.

Moebius, E., et al. (2012), Interstellar gas flow parameters derived from Interstellar Boundary Explorer-Lo observations in 2009 and 2010: Analytical analysis, *Astrophys. J., Suppl. Ser.*, *198*(2), article id. 11; doi:10.1088/0067-0049/198/2/11.

Pryor, W. R., M. Witte, and J. M. Ajello (1998), Interplanetary Lyman α remote sensing with the Ulysses Interstellar Neutral Gas Experiment, *J. Geophys. Res.*, *103*, 26,813–26,831, doi:10.1029/98JA01459.

Pryor, W., et al. (2008), Radiation transport of heliospheric Lyman-α from combined Cassini and Voyager data sets, *Astron. Astrophys.*, *491*, 21–28; doi: 10.1051/0004-6361:20078862.

Quemerais, E., and J.-L. Bertaux (1993), Radiative transfer in the interplanetary medium at Lyman alpha, *Astron. Astrophys.*, *255*, 283–301.

Quemerais, E., J.-L. Bertaux, R. Lallement, M. Berthe, E. Kyrola, and W. Schmidt (1999), Interplanetary Lyman α line profiles derived from SWAN/SOHO hydrogen cell measurements: Full-sky velocity field, *J. Geophys. Res.*, *104*, 12,585–12,603, doi:10.1029/1998JA900101.

Rosenbauer, H., H. J. Fahr, E. Keppler, M. Witte, P. Hemmerich, H. Lauche, A. Loidl, and R. Zwick (1983), The ISPM interstellar neutral-gas experiment, *ESA Spec. Publ., ESA SP-1050*, 123–139.

Rucinski, D., M. Bzowski, and H. J. Fahr (2003), Imprints from the solar cycle on the helium atom and helium pickup ion distributions, *An. Geophys.*, *21*, 1315–1330; doi:10.5194/angeo-21-1315-2003.

Stephan, S., S. Chakrabarti, J. Vickers, T. Cook, D. Cotton (2001), Interplanetary H Lyα observations from a sounding rocket, *Astrophys. J.*, *559*, 491–500; doi: 10.1086/322322.

Tarnopolski, S., and M. Bzowski (2009), Neutral interstellar hydrogen in the inner heliosphere under the influence of wavelength-dependent solar radiation pressure, *Astron. Astrophys.*, *493*, 207–216; doi: 10.1051/0004-6361:20077058.

Thomas, G. E. (1978), The interstellar wind and its influence on the interplanetary environment, *Ann. Rev. Earth Planet. Sci.*, *6*, 173–204; doi:10.1146/annurev.ea.06.050178.001133.

Vallado, D. A. (2001), Fundamentals of Astrodynamics and Applications, Microcosm, El Segundo, Calif., and Kluwer Publ., Dordrecht, The Netherlands.

Wallis, M. K. (1973), Interaction between the interstellar medium and solar wind plasma, *Astrophys. Space Sci.*, *20*, 3–18; doi: 10.1007/BF00645579.

Wallis, M. K. (1974), Local hydrogen gas and the background Lyman-alpha pattern, *Mon. Not. R. Astron. Soc.*, *167*, 103–120.

Wallis, M. K. (1975), Collisional heating of interplanetary gas: Fokker-Planck treatment, *Planet. Space Sci.*, *23*, 419–430; doi:10.1016/0032-0633(75)90116-6.

Wallis M. and M. H. A. Hassan (1978), Stochastic and dynamic temperature changes in the interstellar gas, *Planet. Space Sci.*, *26*, 111–120; doi:10.1016/0032-0633(78)90011-9.

Weller, C. S., and R. R. Meier (1974), Observations of helium in the interplanetary/interstellar wind: The solar-wake effect, *Ap. J.*, *193*, 471–476; doi:10.1086/153182.

Witte, M. (2004), Kinetic parameters of interstellar neutral helium. Review of results obtained during one solar cycle with the Ulysses/GAS-instrument, *Astron. Astrophys.*, *426*, 835–844; doi: 10.1051/0004-6361:20035956.

Witte, M., H. Rosenbauer, E. Keppler, H. Fahr, P. Hemmerich, H. Lauche, A. Loidl and R. Zwick (1992), The interstellar neutral-gas experiment on ULYSSES, *Astron. Astrophys. Suppl. Ser. 92*, 333–348.

Witte, M., M. Banaszkiewicz, and H. Rosenbauer (1996), Recent results on the parameters of the interstellar helium from the Ulysses/GAS experiment, *Space Sci. Rev.*, *78*, 289–296; doi:10.1007/BF00170815.

Witte, M., S. Bleszynski, M. Banaszkiewicz, and H. Rosenbauer (1999), Sputtering efficiency of LiF surfaces on impact of low energy neutral helium 20–80 eV: Calibration of the interstellar neutral helium instrument on ULYSSES, *Rev. Sci. Instrum.*, *70*, 4404–4411; doi: 10.1063/1.1150085.

Wolniewicz, L. (1965), Variational treatment of the HeH^+ ion and the beta-decay in HT, *J. Chem. Phys.*, *43*, 1087–1091,; doi:10.1063/1.1696885.

Wu, F.-M. and D. L. Judge (1978), Electron heating of inflowing interstellar gas, *Astrophys. J.*, *225*, 1045–1049; doi:10.1086/156571.

Wu, F.-M. and D. L. Judge (1979), Temperature and flow velocity of the interplanetary gases along solar radii, *Astrophys. J.*, *231*, 594–605; doi: 10.1086/157221.